Spectroscopy of Amplified Spontaneous Emission Laser Spikes in Phenyloxazoles. Prototype Classes†

Juan Carlos del Valle‡ and Michael Kasha*,§

Institute of Molecular Biophysics and Department of Chemistry, Florida State University, Tallahassee, Florida 32306-3015

Javier Catalán

Departamento de Química Física Aplicada, Universidad Autónoma de Madrid, Cantoblanco 28049, Madrid, Spain

Received: October 25, 1996; In Final Form: January 24, 1997⊗

Ultraviolet amplified spontaneous emission (ASE) laser spikes are demonstrated for the phenyloxazoles. The principal laser spikes are at 333 nm for 2-phenylbenzoxazole (PBO) and at 374 nm for 2,5-diphenyloxazole (PPO), with two laser spikes at 365 and 385 nm for 2-(1-naphthyl)-5-phenyl-1,3,4-oxadiazole (α-NPD), all in hydrocarbon solution at 298 K. The extended symmetrical molecule 1,4-bis(4-methyl-5-phenyloxazol-2-yl)benzene (DPOPOP) has a laser spike at 420 nm. The lasing action is stable with time for stirred hydrocarbon solutions deoxygenated by Ar bubbling. Gain coefficients up to 10 cm^{-1} have been observed in the cases cited. It is demonstrated that the phenyloxazoles can be categorized by the ASE laser spike spectroscopy observed. In the simple case, ASE spike appears at the position of the strongest fluorescence vibronic peak. Phenyloxazoles with asymmetric substitution (PPO, α-NPD) exhibit dual laser spikes, with dominance of that laser spike corresponding to a vibronic band of secondary intensity. This highly anomalous behavior is attributed to two normal mode segments of the electronic systems, with solitonic transfer of vibrational distortion between the segments driven by entropic and energetic preference. It is demonstrated that ASE laser spectroscopy offers excitation dynamics information not revealed in stationary state spectroscopy.

1. Introduction

Phenyloxazoles in various structural modifications (Table 1) generally exhibit a strong first electronic absorption band in the ultraviolet, with a corresponding intense fluorescence band, suggesting the possibility of their use for UV molecular lasers. The molar absorption coefficients are in the range 20 000−25 000, indicating strongly allowed $\pi \rightarrow \pi^*$ lowest singlet-state excitations.

The study of the detailed spectroscopy of amplified spontaneous emission (ASE) and corresponding gain coefficients[1−5] of the substituted phenyloxazoles of Table 1 has revealed a surprising complexity, seemingly violating the simple physical optics principle of ASE laser spike development coincident with the strongest fluorescence emission peak. The explanation of the several anomalies observed led to the realization that the study of ASE laser spike development opens the way to their use as a subtle new tool for the study of the chemical physics of the excitation dynamics of these relatively complex molecular systems. This paper presents a fuller account of our previous communication.[6] Research on the general lasing action of these phenyloxazoles (Table 1) has been reported previously[7−15] in qualitative surveys.

TABLE 1: Classification of Substituted Phenyloxazole Structures

Class 1- Single Skeletal Structure

Main ASE spike coincides with main fluorescence peak, secondary spike suppressed but observed.

Normal gain spectrum relation.

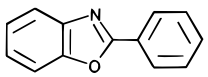

PBO 2-phenylbenzoxazole

Class 2- Symmetrical Double Molecule

Main ASE spike coincides with main fluorescence peak, no other ASE spike appears.

Normal gain spectrum relation.

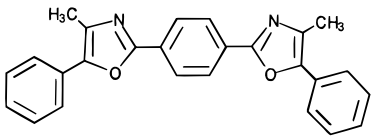

DPOPOP 1,4-bis(4-methyl-5-phenyloxazol-2-yl)benzene

Class 3- Unsymmetrical Composite Molecule

Main ASE spike correlates with main fluorescence peak, subsidiary laser spike anomalously enhanced.

Gain spectra show reversal of intensity ratio.

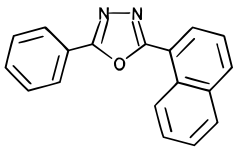

α-NPD 2-(1-naphthyl)-5-phenyl-1,3,4-oxadiazole

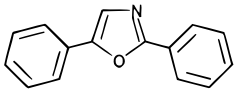

PPO 2,5-diphenyloxazole

Organic molecules in solution acting as lasing media have been studied widely[16,17] since the report by Sorokin and Lankard[18] on the first organic dye laser. The researches traditionally have been carried out using (resonant) mirror cavity

† This paper is dedicated to Professor Robin M. Hochstrasser of the University of Pennsylvania on the occasion of his 65th birthday, in celebration of his many contributions to condensed matter spectroscopy and theory.

‡ Spanish Fulbright Scholar, on leave from Universidad Autónoma de Madrid, Departamento de Química Física Aplicada. Cantoblanco 28049, Madrid, Spain.

§ Work sponsored under Contract DE-FG05-87ER60517 of the office of Health and Environmental Research, U.S. Department of Energy, Washington, DC.

⊗ Abstract published in *Advance ACS Abstracts,* March 15, 1997.

lasers. In contrast, ASE laser spike spectroscopy[1−5] has focused attention on the use of this special technique (ASE lasers, or mirrorless lasers, see below) for evaluation of the absolute efficiency of a laser material.

The study of the spectroscopy of highly resolved ASE laser spikes leads to the possibility of observing multispike phenomena for vibrationally resolved fluorescence spectra. It is natural for a fluorescence Franck−Condon (F−C) envelope with resolved vibronic structure to exhibit initially an ASE laser spike for each prominent vibronic peak, aside from a true 0−0 peak. However, at higher driving laser energy, leading to high gain coefficients (see below), the exponentiality of the subsequent induced emission steps leads to suppression of the minor peaks and development of a main ASE laser spike corresponding to the Franck−Condon maximum in the fluorescence spectrum.

In earlier researches[19] in ASE laser spectroscopy of resolved fluorescence bands, the low gain coefficient ($\alpha \approx 3-5$ cm^{-1}) range did not permit ultimate band narrowing. In more recent work, not only has ASE laser spectroscopy exhibited ultimate band narrowing but the higher resolution has revealed subtleties of response indicating novel internal excitation dynamics features, which are the main subject of this paper.

The laser spectroscopy of phthallocyanine[20] and chlorophyll[21] exhibit normal multiple laser spikes, with the strongest peak correlating with the principal Franck−Condon peak of the fluorescence spectrum and a much weaker secondary laser spike correlating with the lower intensity Franck−Condon fluorescence peak of the minimally resolved vibronic band observed. The authors of both papers label in error the strongest F−C peak as the 0−0 vibronic band, implying a two-level Einstein scheme, which cannot yield population inversion, and hence precludes lasing. However, in these very complex polyatomic molecules, the large number of normal modes of vibration would permit some vibronic transition to develop a F−C peak far enough from an unresolved actual 0−0 band to excite nonequilibrium vibronic levels of the ground state (S_o), yielding the four-level system needed for a laser in such cases.

There is a clear limiting range of multiple laser spike development in the case of molecular *mixtures* in solution. On one hand, the example studied by Chou and Aartsma[22] demonstrated simultaneous ASE laser spikes generated from a molecular mixed solution of the proprietary laser dye bis-MSB and 3-hydroxyflavone, with variation of relative laser peak intensity controlled by the mixture concentration ratio. In this case, the solution mixture exhibited a net fluorescence spectrum with separate fluorescence peaks. On the other hand, using a solution of 1,1,4,4-tetraphenyl-1,3-butadiene mixed with 3-hydroxyflavone, a single new laser spike was observed at an intermediate frequency between the individual laser spikes, which were effectively combined in one resultant spike. In the first case as stated, the combined fluorescence bands exhibited two spectroscopic maxima, whereas in the latter case a single-band fluorescence maximum resulted.

As an example of energy transfer enhancement of laser spike development, we cite the cases of inter- and intramolecular Förster excitation transfer to enhance the laser spike intensity of 9,10-diphenylanthracene[23] and 1,4-bis(4-methyl-5-phenyloxazol-2-yl)benzene[24] (DPOPOP), respectively. This phenomenon will have a strong application with subtle variations in the conclusion of the present paper.

2. Experimental Section

All of the spectroscopic observations were conducted for solutions of the various phenyloxazoles at 298 K in the concentrations and solvents indicated in the text and the figure legends. The absorption spectra were recorded by a Shimadzu UV-2100 spectrophotometer with quartz cuvettes of 1 cm path length. Fluorescence spectra (corrected) were obtained from an AB2 Aminco-Bowman Series 2 luminescence spectrometer. Lifetime measurements were made with the aid of a phase-modulation Fluorolog-2 lifetime spectrofluorometer (SPEX), which modulates the frequency of the excitation light from 0.5 to 300 MHz. The fluorescence lifetimes were obtained relative to glycogen scattering solutions.[25] Decisions on the suitability of the lifetimes rested on examination of the statistics of a fit (a plot of the residual deviations with frequency) and the reduced χ^2 values. The reduced χ^2 values obtained in our experiments were all close to unity.

The ASE laser spike measurements (cf. ref 5) were made by primary excitation with a Nd−YAG laser (Spectra-Physics Model DCR-3G), using the fourth harmonic (266 nm), for all cases except DPOPOP (Table 1), for which the third harmonic (355 nm) was used. The output of the Nd−YAG laser was focused to a narrow line in the dye cell in a transverse geometry. A laser dye cell MOLECTRON DL 251 of 0.8 cm optical path was utilized, which is designed to prevent optical feedback from the windows. The dye solution was stirred to eliminate secondary processes (e.g., local heating, triplet population, etc) from interfering with the experiments. The amplified spontaneous emission (ASE) was dispersed by a 300 lines/mm, 0.32 m polychromator (Instruments SA Model HR320) and detected by an optical multichannel analyzer (OMA) system consisting of an intensified silicon photodiode array (EG & G /PAR, model 1421), and analyzed by a system processor (EG & G /PAR, model 1461/1463). To reduce the noise, the detector was operated in gated mode synchronously with the Nd-YAG laser. The ASE was detected through a pinhole 0.05 cm in diameter placed at a distance of 50 cm from the sample cell.

In the laser experiments, the solutions were degassed by bubbling Ar gas through the working solution in the ASE laser cell for 30 min prior to excitation. It should be emphasized that the laser spikes and their respective gain coefficients were measured in a mirrorless laser cavity without feedback from the windows of the cuvette.

The lifetime, fluorescence, and ASE experiments were carried out by monitoring the light from the sample in a right-angle arrangement in the instruments used with the respective excitation source. This arrangement tends to maximize self-absorption effects, most notable at the higher concentrations employed in the ASE determination.

Photoinstability of the sample was negligible during the experimental time. Photostability of the compounds studied was demonstrated by monitoring the absorption spectra before and after the laser experiments, using a cuvette of 0.01 cm optical path length.

In order to measure the gain coefficient values, a half-cell shutter is placed between the primary laser excitation and the cell to block half the excitation beam. The intensities of the primary laser excitation at the respective full-cell width and half-cell width of the shutter were optically calibrated with a volume absorbing disc calorimeter (Scientech, Inc., Model 36-0001).

The molecules PBO and PPO (see Table 1) were purchased from Aldrich Chem. Co. The compounds α-NPD and DPOPOP were acquired from Lancaster Synthesis, Inc., and Eastman Kodak Co., respectively. All of the compounds were 99% pure and used as supplied.

To confirm purity, ^{13}C-NMR spectra were recorded at 298 ± 2 K on a Bruker/IBM WP270SY NMR spectrometer at 67.932 MHz. Chemical shifts (ppm) were measured in per-deuterated chloroform ($CDCl_3$). The $CDCl_3$ (77 ppm) was used

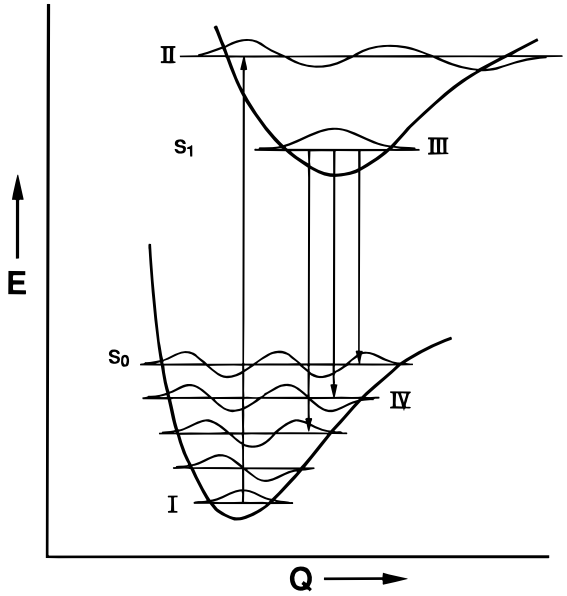

Figure 1. Schematic potential function diagram for a four-level molecular band laser. The I and III states are the lowest vibronic energy levels of S_o and S_1, with the nonequilibrium Franck−Condon vibronic levels of S_1(II) and S_o(IV) serving as the second and fourth states, respectively.

as internal secondary standard relative to TMS. The ^{13}C-NMR spectra of PPO and α-NPD showed 11 and 16 peaks, respectively, which were assignable to the 11 and 16 nonequivalent C atoms. No other significant signals accounting for impurities were found. These results are particularly important because of the suggestive behavior of these two molecules as dual molecular structures. The ^{13}C-NMR spectra confirm the relative purity of the samples used.

The melting point temperatures were measured from the peak melting endotherms using a Perkin-Elmer DSC 2B differential scanning calorimeter at a heating rate of 10 K/min. The melting temperatures for α-NPD and PPO were determined to be 123.4 and 73.3 °C, respectively. These data allow us to estimate their purity to be higher than 99%.

All the solvents used were spectrophotometric grade.

The theoretical calculations of the 2-phenyloxazole and 5-phenyloxazole molecules were carried out for both the ground electronic state (S_o) and the lowest excited singlet electronic state (S_1), whose geometries were optimized using a 6-31G** basis set with the Gaussian 94[26a] program. The S_o geometry was calculated at the self-consistent field (SCF) level, and the S_1 geometry was obtained by means of a CIS method[27] due to the size of our systems. Calculations for the molecule 2,5-diphenyloxazole (PPO) were done only for the S_o state. The S_1 state for PPO was not calculable owing to insufficient computer memory. The torsional energy barriers were calculated using the final optimized geometry of each molecule (which was planar), by freezing the molecule at a given inter-ring angle and thereby performing the calculation without further optimization of the geometry. The Spartan 4.1 program[26b] was used for visualizing the vibrational modes. The harmonic vibrational frequencies (cm^{-1}) were multiplied by a scaling factor of 0.8953.[28]

3. The Two-State/Four-Level (Continuous Molecular Band) Laser

In the absence of auxiliary excitation mechanisms,[29] such as proton-transfer (PT) tautomerism or twisting-intramolecular-charge transfer (TICT) excitations, the two-state/four-level molecular band laser scheme[30] would be applicable (Figure 1) for possible laser excitation.[31] This scheme is the one well recognized for the mechanism of laser dyes in general.[3] In this scheme, levels I and III are the zero-point vibronic levels corresponding to the usual singlet electronic states commonly existing, S_o and S_1. The vibronic levels II and IV represent the (thermally) nonequilibrium vibronic levels of the respective states S_1 and S_o, excited in the electronic transition. The levels II and IV may lie within a continuous Franck−Condon envelope for the corresponding absorption and fluorescence or may represent partially resolved vibronic bands. The nonequilibrium levels II and IV are excited as probable Franck−Condon transitions and are rapidly equilibrated by intramolecular vibrational relaxation (IVR). Ricard et al. have measured the IVR thermalization to be on the short picosecond time scale.[32]

A population inversion can be produced for the zero-point level of the electronic state S_1 relative to the nonequilibrium F−C levels of S_o. The key requirement for a four-level molecular band laser to be operative efficiently is for the upper potential surface minimum to suffer a major displacement from the S_o potential minimum. In the schematic vibrational potential shown in Figure 1, it could be assumed that the displacement is for a large skeletal distortion of the excited molecule. In large polyatomic molecules a more common origin of a large potential minimum displacement is a torsional mode, in which large amplitude internal twisting occurs with respect to a bond axis with a strongly displaced excited state minimum. Alternatively, a change of skeletal conformation[33] from S_o to S_1, would permit a four-level molecular band scheme to be operative.

A strong possibility can exist in the four-level molecular band laser for self-absorption of the fluorescence. This self-absorption is conditioned by the overlap of the origins of the strong first absorption band and the fluorescence band. This possibility must be monitored in a critical way. This is a special point of caution because the fluorescence spectroscopy of the present series of molecules requires very dilute solutions (e.g., 5×10^{-6} M), for an authentic fluorescence Franck−Condon profile to be observed, whereas the ASE laser spike spectroscopy usually involves rather more concentrated solutions (e.g., 0.005 M).

The general result of this study is to show that, in the class of molecules (Table 1) with a definable single electronic system enveloping a single skeletal structure (class 1), a normal lasing behavior is found, with a single dominant ASE laser spike correlated with the principal F−C fluorescence peak. Of course, the 0−0 vibronic transition cannot give rise to an ASE laser spike.

In the present case of phenyloxazole molecules with unsymmetrical substituents about the oxazole nucleus, a completely unorthodox behavior is observed, in which the ASE laser spike for the dominant F−C fluorescence peak is *suppressed* and a weaker subsidiary F−C peak is *enhanced*. Investigation of this phenomenon in a later section of the paper shows that increasing laser energy and molecular concentration enhances the anomaly. The analysis requires that not only must we assume intramolecular vibronic energy transfer occurs between two sets of molecular species within the overall complex molecule, behaving as a molecular mixture, but also that intermolecular transfer of excitation energy becomes prominent. The behavior is analogous to the twin ASE laser spike development[22] for mixtures of separate laser molecules. We consider our system to consist of a molecular mixture of two different vibratory electromers, which we identify with different normal-mode segment (cf. Scheme 1) partitioning of the unsymmetrical composite molecule and having a common electronic state. Then, we show how, in the excitation dynamics under laser

SCHEME 1: Model of Partitioning of Composite Molecules into Molecular Segments or Vibratory Electromers

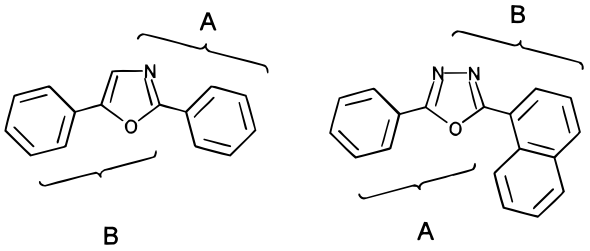

excitation, the excess vibronic excitation can be redistributed intra- and intermolecularly between the vibrating electromers, leading to a dominant ASE laser spike for an apparently weaker subsidiary fluorescence band masked by the net spectrum of the composite molecule.

4. Amplified Spontaneous Emission Spectroscopy

A cavity laser, with the mirror enhancement of coherence (Figure 2), acts as a power amplification laser exhibiting a coherent radiation beam. Although coherent lasers are commonly used and understood, the deliberate generation of coherency by the cavity components and structures that serves to boost the radiation power is antithetical to the use of the cavity laser for evaluating the *efficiency* of amplification as a function of frequency. Therefore, the special antiresonance cell used in amplified spontaneous emission[1−5] (ASE) spectroscopy must be applied. Because this technique is not widely practiced, a few words of explanation are given here (Figure 2). In the ASE cell no mirrors are used, and the exit windows are set obliquely to the photon emission path so that no optical resonances are set up at any frequency. Wave trains of successive induced emissions can originate at any point and consequently the exit laser beam is macroscopically incoherent. It is to be noted that the terms (macroscopically) *incoherent* and *laser* are not literally mutually exclusive, as paradoxical they may seem in relation to the concept of a cavity or coherent laser. This type of laser has also been named as an ASE laser or mirrorless laser and with some additional conditions a superradiant laser (cf. ref 34). The ASE laser output characterizes the intrinsic molecular laser frequency spectrum. An acoustical analog of the ASE mirrorless laser is the anechoic (zero-echo) chamber for recording of faithful acoustical power vs frequency spectra; in contrast, a resonant chamber boosts some frequencies dependent on standing waves, analogous to the typical action of a cavity laser.

Between the primary excitation laser and the ASE cell is placed a half-cell shutter, optically calibrated to block half the excitation beam intensity. Then, the nonlinearity of the exit beam intensity under variation of cell length can be measured as a function of the intensity ratio $I_L/I_{L/2}$. For a highly efficient laser material, a ratio of ca. 60 or more can be observed (cf. Figure 3), leading to a gain coefficient value of $\alpha = 10$ cm^{-1} (reciprocal cell length units, not wavenumbers) by the equation[1,3]

$$\alpha(\lambda)_L = \frac{2}{L}\ln\left[\frac{I_L}{I_{L/2}} - 1\right]$$

In this determination, a pinhole aperture (e.g., 0.05 cm at 50 cm from the cell window) is a crucial requirement for efficient sampling of a uniformly homogeneous laser beam with regard to maximum number of induced emission steps. A linear excitation condition would of course yield the beam intensity ratio $I_L/I_{L/2} = 2$. A series of six consecutive steps of induced emission (with photon doubling at each step) would lead to an $I_L/I_{L/2}$ ratio of 64. The gain coefficient α has dimensions of L^{-1} or cm^{-1}. The cell used in the current research has a path length L of 0.80 cm.

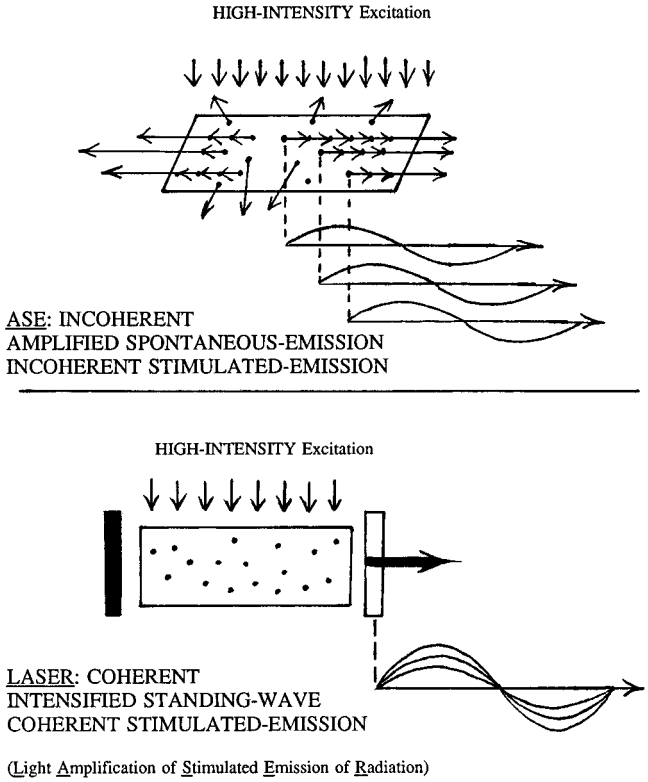

Figure 2. Diagram contrasting the coherent cavity laser with the amplified spontaneous emission (ASE) laser, which generates a macroscopically noncoherent laser beam but permits the gain coefficient α to be measured for the exponentiality of successive photon multiplication.

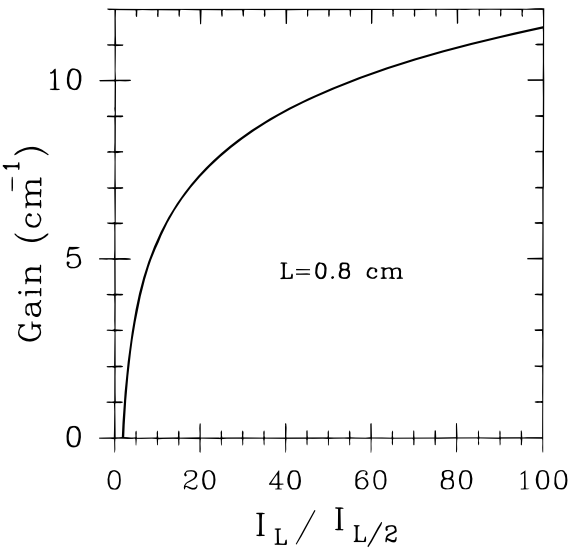

Figure 3. Amplified spontaneous emission (ASE) gain coefficient α as a function of cell/half-cell ($I_L/I_{L/2}$) beam intensity of the dye laser.

The laser gain coefficient can be given for the ASE laser spike maximum, or conversely $\alpha(\lambda)_L$ can be plotted as the gain spectrum over the useful observable wavelength range of α. Such a gain spectrum offers information on laser tunability range and on intra- and intermolecular energy transfer in suitable molecular systems.

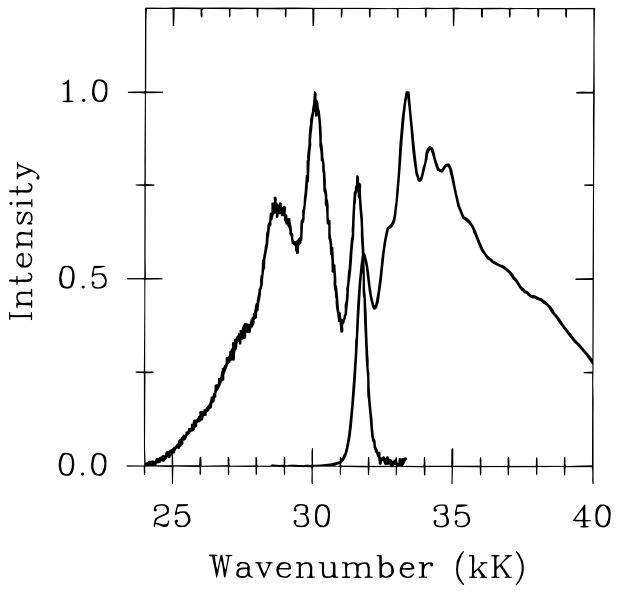

Figure 4. Absorption and fluorescence spectrum of 2-phenylbenzoxazole (PBO, Table 1) in methylcyclohexane solution at 298 K (1.5×10^{-6} M) plotted vs frequency in kilokayser (kK). One kilokayser is equal to 1000 cm^{-1}.

5. Absorption Spectra of the Phenyloxazoles

The absorption curves for the phenyloxazoles of Table 1 are given in Figures 4 and 5 for hydrocarbon solution at 298 K. In the case of 2-phenylbenzoxazole (PBO), the absorption curve shows somewhat more vibronic complexity than does the fluorescence emission. This additional complexity, and the relatively greater bandwidth of the absorption band indicates the presence of at least one more electronic transition within the band. Strong absorption−fluorescence overlap in the 0−0 band occurs, but because of the relative sharpness of the band structure, the overlap does not extend far into the fluorescence band. Progressive suppression of the fluorescence 0−0 band by self-absorption is observed by increasing the concentration, but as this band is not active in lasing action, this feature does not affect the ASE laser spike results significantly. The self-absorption can be reduced by front-face illumination, but in the ASE spectroscopy this is not possible, and the self-absorption for the more concentrated solution used in ASE spectroscopy may shift the ASE laser spike slightly.

The absorption spectra for the other phenyloxazoles of Table 1, 1,4-bis(4-methyl-5-phenyloxazol-2-yl)benzene (DPOPOP), 2-(1-naphthyl)-5-phenyl-1,3,4-oxadiazole (α-NPD), and 2,5-diphenyloxazole (PPO) shown in Figure 5 appear as highly diffuse bands with little vibronic resolution. The first or lowest energy UV absorption bands for these molecules represent overlapping electronic absorptions to both torsional modes and stretching normal modes and exhibit a complexity, diffuseness, and enhanced bandwidth. In contrast, the half-width of the fluorescence band of the molecules studied is smaller and the vibrational structure substantially better resolved. The fluorescence spectrum originates in transitions at the potential minimum of the upper state with little torsional excitation.[35] The torsional modes are strongly medium controlled,[35] and in comparing the 77 K spectra of PBO, DPOPOP, PPO, and α-NPD the vibrational structure of the fluorescence and absorption spectra are remarkably similar in the classical Levshin[36] mirror image relation.

The absorption coefficients at the highest peak for each of the "first band regions" are all in a high range, with log ϵ values in methylcyclohexane of 4.31 (292 nm), 4.74 (363.5 nm), 4.21 (314 nm), and 4.46 (309 nm), respectively for PBO, DPOPOP, α-NPD, and PPO (Table 1). These high values of absorptivity imply strong self-absorption in the onset region of the fluorescence spectra, which may reflect itself in the wavelength position of the ASE laser spike.

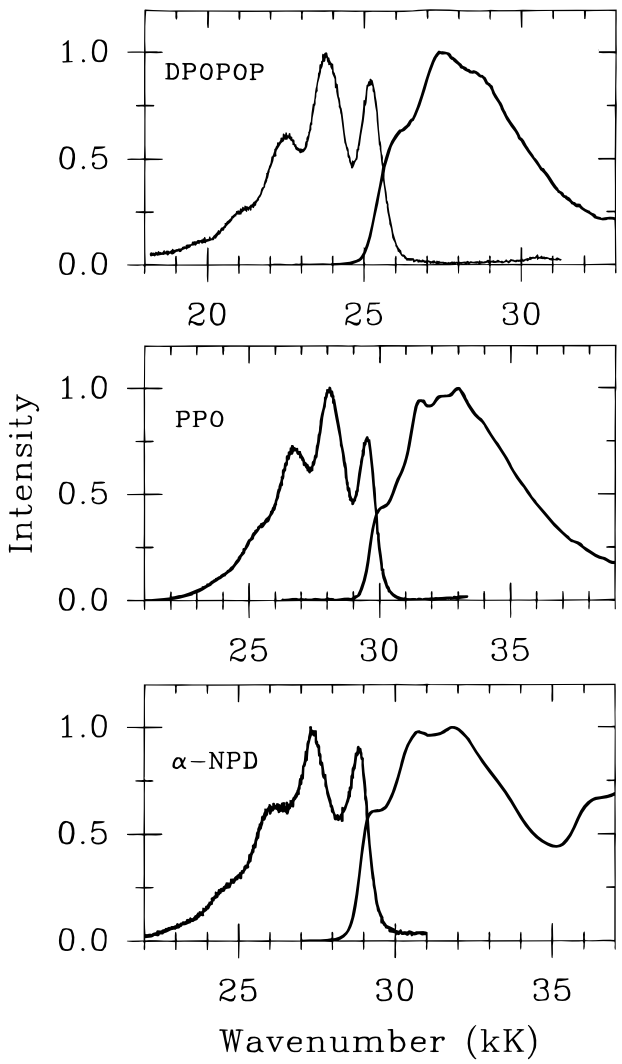

Figure 5. Absorption and fluorescence spectra of DPOPOP, PPO, and α-NPD in methylcyclohexane at 298 K. One kilokayser (kK) is equal to 1000 cm^{-1}.

6. Fluorescence, Lifetimes, ASE, and Gain Spectra of Phenyloxazoles

A correlation of the molecular structural types of the phenyloxazoles under study in the present research (Table 1), with the variation of amplified spontaneous emission (ASE) laser spike behavior relative to the corresponding fluorescence spectra, led us to classify the molecules into three separate groups.

Class 1. This is the normal case in which the ASE laser spike correlates with the strongest Franck−Condon vibronic band observed in the fluorescence spectrum, discounting a possible 0−0 band.

The molecule PBO represents a prototype for this case and is known[7,33,37] to exist as a single conformer. The electronic structure covers the whole skeletal domain, with the 2-phenyl ring conjugated and coplanar with the benzoxazole moiety. The lowest electronic transition is directly assignable as a $\pi \rightarrow \pi^*$ lowest $S_o \rightarrow S_1$ transition, with whole skeletal normal modes of vibration. As previously reported,[6] the PBO phase-modulation data fit a single-term exponential decay, with a mean

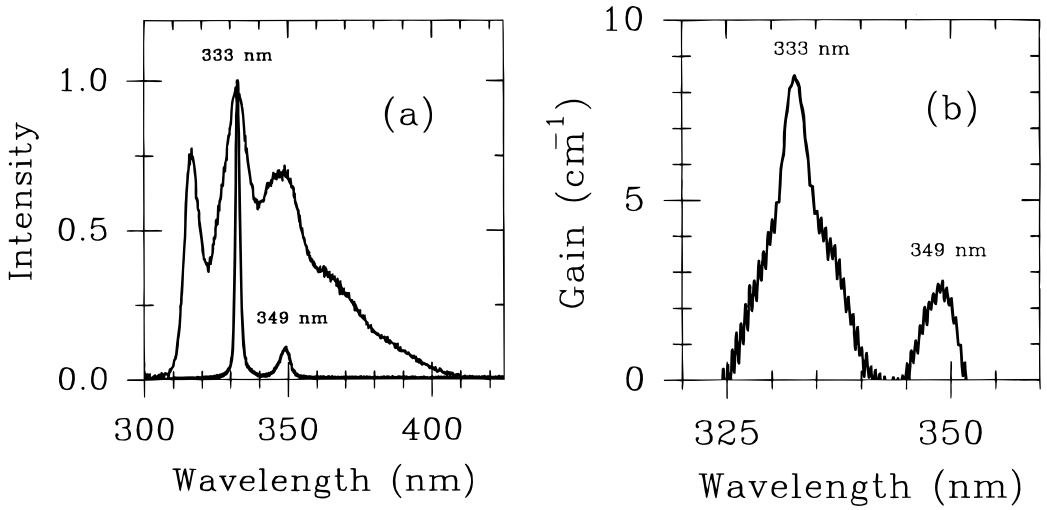

Figure 6. (a) Fluorescence (1.5×10^{-6} M) and ASE (0.0055 M) laser spike spectrum for 2-phenylbenzoxazole in methylcyclohexane at 298 K. (b) Gain spectrum for 2-phenylbenzoxazole (0.0055 M) in methylcyclohexane at 298 K in a 0.8 cm ASE cell. The gain coefficient α for the second vibronic band is 8.5 cm^{-1}, and for the third band the α coefficient value is 3 cm^{-1}. The α coefficient values are in reciprocal cell length units. Nd−YAG laser pulse energy was 5 mJ. (cf. Figure 10).

lifetime of 1.27 ± 0.03 ns in 1.0×10^{-5} M solution in methylcyclohexane upon excitation at 266 nm.

The well-developed vibronic structure of the fluorescence spectrum (Figure 4) of 2-phenylbenzoxazole in methylcyclohexane gives rise to two ASE laser spikes (Figure 6a), the strongly dominant one appearing at 333 nm the weaker subsidiary spike at 349 nm correlating with the second most intense Franck−Condon fluorescence band, disregarding the 0−0 band.

The relative apparent fluorescence vibronic intensities for the methylcyclohexane solution of PBO have an intensity order band sequence 2 > 1 > 3 (Figure 6a), with the 0−0 band clearly defined as band number 1. Thus the main ASE laser spike corresponds to band 2 and the much weaker spike to band 3, whose laser spike has 0.1 times the intensity of the dominant laser spike correlating with band 2 (the fluorescence band intensities for 2 and 3 being 1−0.7).

Figure 6b presents the gain spectrum of the 2-phenylbenzoxazole molecule, showing two maxima at the same wavelength position as those of the corresponding vibronic bands of the fluorescence. A high gain coefficient value of 8.5 cm^{-1} is achieved at 333 nm.

In the simple excitation case for class 1, the excitation mechanism for development of the ASE laser spikes can only be the four-level laser scheme illustrated in Figure 1. The smaller gain coefficient associated with the weaker fluorescence vibronic bands leads to suppression of the subsidiary ASE laser spikes. At very high gain coefficient approaching α-values of 10 cm^{-1} or higher, the subsidiary spikes may be completely suppressed. At the lowest driving laser energy yielding population inversion, a gain coefficient α of 3 to 5 cm^{-1} may be observed. In such a case, the ASE laser spike intensities tend to mimic the fluorescence vibronic band intensities as a limit.

Class 2. This case is expected for a composite (dual) molecule, in which two equivalent moieties are very weakly coupled electronically or are electronically isolated. If the lowest $S_o \rightarrow S_1$ absorption is very strong, and the intercenter distance of the two molecules is in the range of molecular diameters or slightly greater (e.g., 5−10 Å), the strong-coupling molecular exciton model should apply.[38−40] Although usually it is a severe test for the point−dipole approximation to be used in such extended molecules, in the present case the intermolecular centers are about twice the molecular diameter. The molecular exciton model then can give an order of magnitude expected for electronic displacement of the "dimer" states from the component single-molecule lowest transition energy. If the case of oscillatory excitation between *equivalent* electronic units in the molecules is operative, the single-molecule Franck−Condon vibronic pattern would be displaced by the molecular exciton dipole−dipole coupling (strong coupling case).[41,42] In laser excitation, the consequence could be a uniquely appearing ASE laser spike (for the appropriate exciton selection rule).

The molecule DPOPOP at first sight would appear to fit this class 2 molecular skeletal description. This molecule (Table 1) could be considered as consisting of a pair of 5-phenyloxazole groups coupled by an intercalating *p*-phenyl link at the respective oxazole 2 positions. We could consider, in such a case, that the 5-phenyloxazole moieties could be essentially coplanar electronic units with intrinsic normal vibrational modes, then weakly coupled as a result of torsion about the 2-oxazole bonds to the intervening phenyl group.

Molecular Exciton Calculations. Using this model, we could test the action of dipole−dipole coupling[41] between two 3-methyl-5-phenyloxazole groups by the strong-coupling Davydov molecular exciton model.

We carried out the calculations using the experimental results for 2-phenyloxazole in methylcyclohexane, because 3-methyl-5-phenyloxazole was not commercially available. This took into account our ab initio calculations (see Experimental Section), which show that the electronic transition $S_1 \rightarrow S_o$ for 2-phenyloxazole and 5-phenyloxazole are very close in energy and oscillator strength, i.e., 262.1 nm ($f = 0.72$) and 264.2 nm ($f = 0.74$), respectively. Thus, by applying the equation $f = 4.32 \times 10^{-9} \int \epsilon \, d\bar{\nu}$ an *f*-number value of 0.54 was calculated. The corresponding transition moment is 5.5 D ($|M^2| = f / [4.74 \times 10^{29} \bar{\nu}]$) and the dipole−dipole interaction energy (ϵ) can be obtained from the equation $\epsilon = -f / [4.74 \times 10^{29} \bar{\nu} R^3]$ where $\bar{\nu}$ is the wavenumber at the absorbance maximum of the first electronic transition for 2-phenyloxazole in methylcyclohexane (at 38 000 cm^{-1}). Assuming a 9 Å distance (*R*) between the centers of gravity of the two phenyloxazole units, the dipole−dipole energy interaction would range from about −230 to −460 cm^{-1} for orientations between dipoles from a parallel dimer type to a tail-to-head dimer type, respectively. We estimate that a displacement of ±230 cm^{-1} would be expected, taking into account the position of the shifted electronic bands of a "dimer"

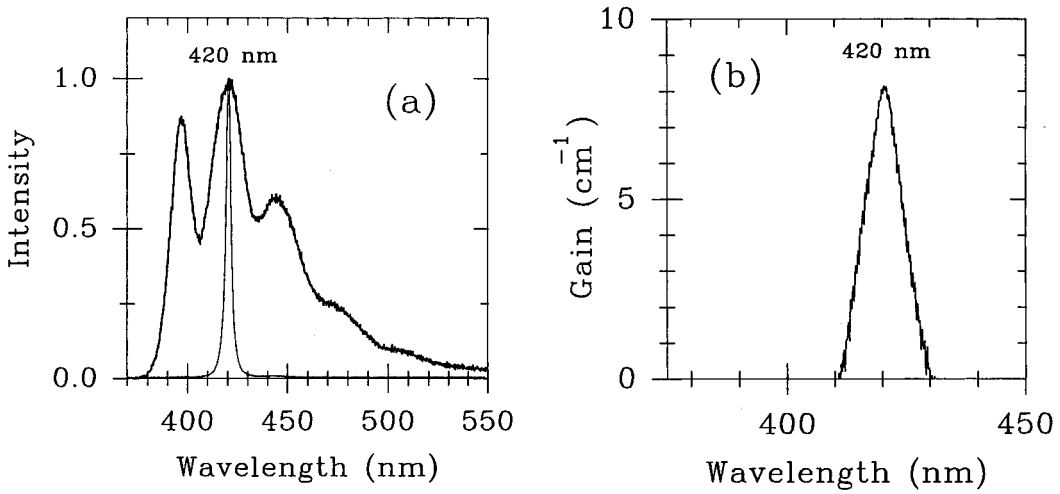

Figure 7. (a) Fluorescence (0.5×10^{-6} M) and ASE (0.000 31 M) of DPOPOP in methylcyclohexane at room temperature. It shows an ASE spike at 420 nm. (b) Gain spectrum in cm^{-1} (reciprocal cell length) of the DPOPOP molecule (0.00031 M) in methylcyclohexane at room temperature. Nd:YAG laser pulse energy was 5 mJ.

or double molecule in relation to the undisplaced position of the first UV $S_o \rightarrow S_1$ band of the single 2-phenyloxazole molecule (at 291 nm). The estimated 0−0 first UV absorption band for 3-methyl-5-phenyloxazole would occur at ca. 293 nm, verifying that the DPOPOP with its $S_o \rightarrow S_1$ 0−0 transition observed at 391 nm does not seem to have the skeletal conformation required for the dimer molecular exciton interaction.

The steric hindrance of the 3-methyl group on each 5-phenyloxazole probably prevents an intrinsic planarity of these 5-phenyloxazoles, strongly limiting electronic conjugation within the group, and limiting the development of strong electronic absorption for the 5-phenyloxazole groups as a unit.

The DPOPOP molecule could be structurally modified to permit excitonic dipole−dipole coupling by (a) the replacement of the two 4-methyl groups on the oxazole rings by H-atoms and (b) the introduction of two methyl groups at the 2,3 positions on the central 1,4-phenyl ring. This would serve to electronically decouple the central three rings as described below and would permit the pair of 5-phenyloxazole rings to undergo excitonic dipole−dipole coupling upon excitation.

An alternative DPOPOP skeletal structure that suggests itself, accepting the enforced torsion of the two 5-phenyl groups to be out-of-plane with the attached oxazole ring, is to assume coplanarity (and strong electronic conjugation) within the 3-ring oxazole−phenyl−oxazole central core of the molecule. This skeletal model is qualitatively consistent as an extended electronic system with a wavelength shift from 330 nm (cf. PPO, Table 1) to 380 nm for DPOPOP, measured by the fluorescence onsets (Figures 9a and 7a, respectively).

The fluorescence spectrum for DPOPOP (3.6×10^{-6} M) at room temperature and the ASE laser spike spectrum (3.1×10^{-4} M), both in methylcyclohexane, are given in Figure 7a. The ASE laser spike for DPOPOP coincides with the dominant 2nd fluorescence band observed at 420 nm and is narrow and unique with no sign of auxiliary vibronic band contribution. The gain spectrum for this molecule (Figure 7b) exhibits a unique peak with $\alpha = 8.2$ cm^{-1} at the position (420 nm) of the ASE laser spike. The 0−0 band is the second-most intense band and cannot give rise to a laser spike as indicated previously. Thus, the suppression of the ASE laser spike from the relatively weaker third fluorescence band is easily achieved.

The phase-modulation data for DPOPOP fluorescence in 5.7×10^{-6} M solution in methylcyclohexane fit a single-term exponential decay with a mean lifetime of 1.18 ± 0.02 ns. These lifetime experiments were carried out upon excitation at 354 nm and by monitoring the fluorescence at 400, 420, 440, or 470 nm.

Class 3. This class covers unsymmetrical composite molecules with inequivalent component segments, which exhibit anomalous ASE laser spike development, usually manifested as a dominant ASE spike correlating with a secondary weaker vibronic peak instead of with the dominant vibronic peaks of a resolved fluorescence band. The gain spectrum for these cases shows corresponding inversion of intensities, with a disproportionately larger gain spectrum peak at the position of the anomalously intense ASE laser spike. This behavior suggests intramolecular and intermolecular vibronic energy transfer in the system. The anomalous behavior is distinctively corroborated by the relative ASE laser spike development under increasing driving laser energy. This aspect will be dealt with in the next section of this paper.

The molecule α-NPD (Table 1), is an example of a class 3 molecule. The absorption and fluorescence spectra of this molecule (Figures 5 and Figure 8a) would appear to be those for a simple case analogous to that for PBO (Class 1). The partially resolved fluorescence vibronic structure superficially represents an ordinary electronic−vibronic transition. Furthermore, α-NPD fluorescence also has a single-term mean lifetime (1.51 ± 0.03 ns) in 2.2×10^{-5} M solution in methylcyclohexane, upon excitation at 266 nm. The mean lifetime is independent of the monitoring wavelength used in our experiments (at 350, 370, 390, or 410 nm).

The ASE laser spike spectrum for α-NPD (Figure 8a) immediately indicates complexity in the excitation dynamics of this molecule. The third most intense fluorescence vibronic band gives rise to an extraordinary intensity for the corresponding ASE laser spike compared to the behavior of a simple molecule.

The gain spectrum for α-NPD (Figure 8b) emphasizes the anomaly present for this molecule. The unusual prominence of the gain peak corresponding to the anomalous ASE laser spike indicates the presence of an unusual amplification process acting in this case.

In contrast to the appearance of the normal absorption and fluorescence spectra for α-NPD, which seems to behave like a simple, single-species molecule, the ASE laser spike and gain spectra show that α-NPD simulates the behavior of a molecular mixture. The ASE laser spike development for molecular mixtures has been explored by Chou and Aartsma[22] as discussed

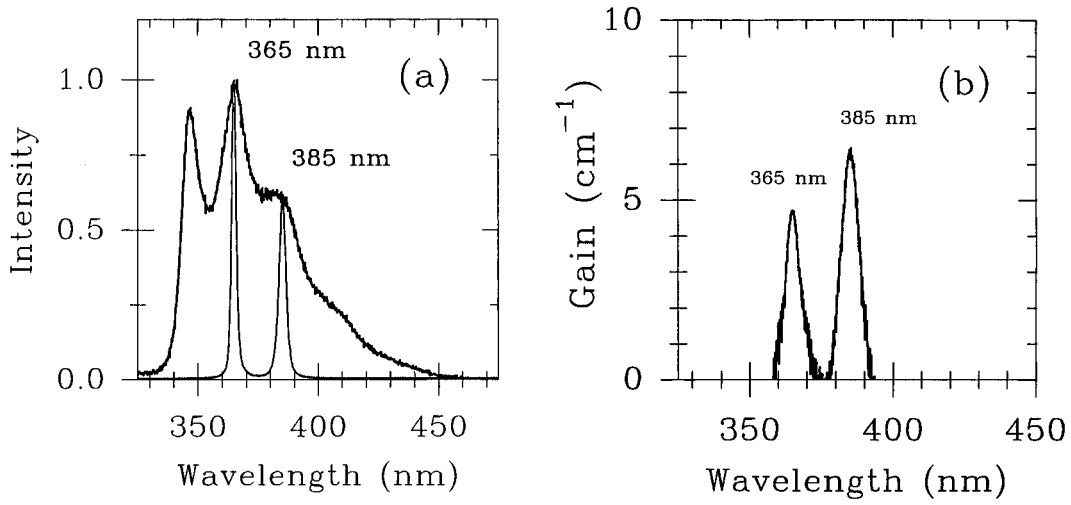

Figure 8. (a) Fluorescence (1.8×10^{-6} M) and ASE (0.0050 M) spectra of the α-NPD molecule in methylcyclohexane at room temperature. The ASE spike maxima are localized at 365 and 385 nm. (b) Gain spectrum of α-NPD (0.0050 M) in methylcyclohexane at room temperature. Nd:YAG laser pulse energy 20 mJ. (cf. Figure 11).

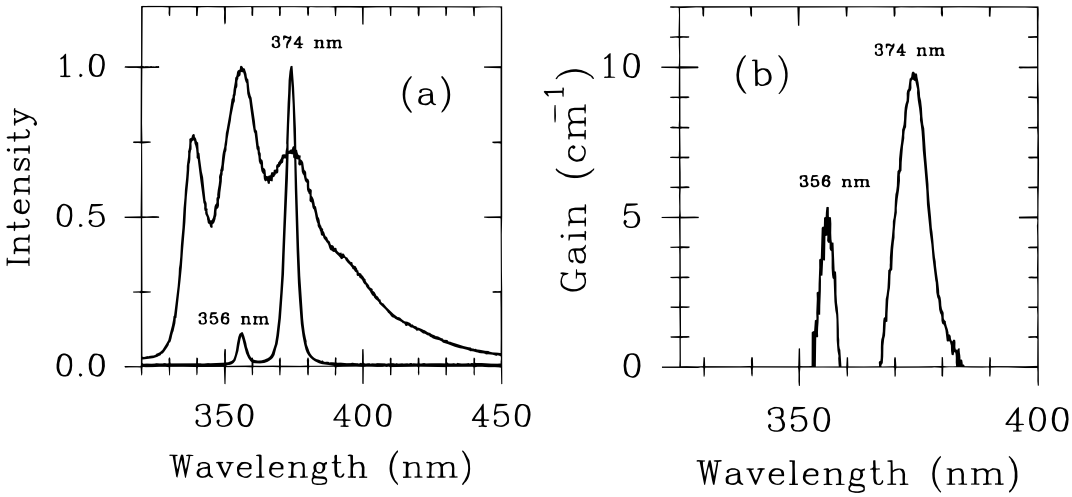

Figure 9. (a) Fluorescence (6.9×10^{-6} M) and ASE (0.0053 M) spectra of PPO in methylcyclohexane at room temperature. The ASE laser maxima are localized at 356 and 374 nm. Nd−YAG laser pulse energy was 20 mJ. (cf. Figure 12). (b) Gain spectrum of PPO (0.0053 M) in methylcyclohexane at room temperature.

earlier. A molecular mixture exhibiting resolved fluorescence peaks is capable of yielding separate ASE laser spikes, with interchange of intensities proportional to the species concentration.

As a model to fit the highly unorthodox ASE laser spike behavior of α-NPD, we define a special class of molecular conformers. We introduce the idea of *normal mode electromers* defined as follows: (a) the normal mode systems consist of two (mechanically) decoupled parts, each having independent normal modes, the coplanar segment and the complementary out-of-plane ring and (b) the electronic wave function envelops the entire molecular skeleton, giving rise to whole-skeleton electronic states. We take our prototype for the latter in such molecules as biphenyl, which in spite of a considerable equilibrium inter-ring twist of some 22°, nevertheless exhibits whole-molecule electronic states. We shall discuss the excitation dynamics of this model in section 8.

Segment A contains an analogue of a 2-phenyloxazole in that the phenyl H-atoms at the 2,6 positions can interact with the lone-pair orbitals on the oxazole N- and O-atoms, suggesting planar stabilization by weak H-bonds. Segment B coplanarity can be destabilized in the ground state by hydrodynamic forces acting on the large molecular plane of the naphthyl group.

The composite nature of α-NPD can be considered by segmenting into special molecular conformers as follows (Scheme 1). Segment A is taken as the 5-phenyl ring coplanar with the 1,3,4-oxadiazole, with the 1-naphthyl lying out-of-plane by torsion about the 2 position of the oxadiazole ring. In the other special conformer, the phenyl group lies twisted out-of-plane and the 1-naphthyl group is coplanar with 1,3,4-oxadiazole ring to which it is attached at the 2 position; we consider this coplanar fragment as segment B.

The molecule PPO (Table 1) offers a second dramatic example of a class 3 molecule. The fluorescence spectrum (Figure 9a) for PPO at room temperature, 6.9×10^{-6} M solution in methylcyclohexane (cf. Figure 5), has the appearance of a normal simple molecule fluorescence behavior. However, as Figure 9a shows, the ASE laser spike is strikingly anomalous, the dominant spike correlating with a weaker fluorescence vibronic band, while the strongest Franck−Condon fluorescence vibronic band yields a weak subsidiary ASE laser spike.

The gain spectrum (Figure 9b) for PPO emphasizes the anomalous amplification behavior. Again, the ordinary electronic absorption and fluorescence spectra for the molecule PPO correspond to the simplest molecular behavior, whereas the ASE

laser spike spectrum and gain spectrum correspond to the behavior of a molecular mixture.

It is well-known that PPO generates excimers[43,44] in highly concentrated solutions. For example, for the PPO monomer in xylene solution[43] at room temperature a mean fluorescence lifetime of 2.65 ns is observed. The PPO excimer in 0.45 M xylene solution[43] at room temperature exhibits a fluorescence mean lifetime of 14.0 ns. However, in our experiments, the profile of the PPO fluorescence in methylcyclohexane does not show any variation accounting for an excimer emission on increasing the concentration from 1.0×10^{-6} to 5.9×10^{-3} M (266 nm excitation with a high-pressure xenon lamp). For the 1.0×10^{-6} M solution, a lifetime of 1.23 ± 0.03 ns was obtained corresponding to a single-term exponential decay. The resultant lifetime value is invariant on using the monitoring wavelengths of 345, 365, 385, and 415 nm. The mean lifetime measured for the 5.9×10^{-3} M solution was 2.60 ± 0.05 ns, obtained by observing the fluorescence either at 345 or at 355 nm. In contrast, a lifetime of 3.1 ± 0.1 ns is measured for the fluorescence monitored at any of the following wavelengths: 365, 375, 385, and 415 nm. Therefore, there is no evidence of excimer fluorescence emission in our experiments on PPO solutions as the observed lifetimes are 5 times shorter than the lifetime for the excimer. However, the analysis of the mean lifetimes measured in 5.9×10^{-3} M solution suggests an energy transfer from PPO molecules fluorescing at shorter wavelengths (e.g., 345 and 355 nm) to molecules fluorescing at longer wavelengths (e.g., 365, 375, 385, and 415 nm). The lifetime delay obtained at the highly concentrated solution in comparison with the dilute solution likely is caused by radiation trapping in such strongly absorbing molecular systems, conditioned probably by radiative intermolecular energy transfer.

The PPO molecule (Table 1) we consider for the purpose of our model to exist as a special conformer distinguished by molecular segment partitioning (Scheme 1): Segment A consisting of a coplanar 2-phenyloxazole coupled at the 5 position to a phenyl ring lying twisted out-of-plane and *segment B*, a coplanar 5-phenyloxazole, coupled at the 2 position to a phenyl ring, lying twisted out of plane.

Segment A corresponds to the coplanar 2-phenyloxazole structure, probably stabilized by two weak H-bonds between the 2,6 position H-atoms, overlapping the field of the lone-pair orbitals of the neighboring N- and O-atoms. Segment B coplanarity is reduced by the H-atom repulsion between the 2 position H-atom on the phenyl ring and the 4 position H-atom on the oxazole ring.

As in the case of α-NPD, we consider that the electronic states correspond to electronic wavefunctions enveloping the whole molecular skeleton, whereas the coplanar segments and the out-of-plane ring have decoupled normal modes of vibration. These define the type of conformers we label as *normal mode electromers.*

7. Discriminating Test of ASE Laser Spikes via Driving Laser Energy

In the last section it has been demonstrated that ASE laser spectroscopy offers a tool for the study of excitation subtleties that are not revealed by ordinary equilibrium absorption and fluorescence spectroscopy. In this section it will be shown in addition that variation of driving laser energy can serve to discriminate between normal ASE laser spike development and unorthodox ASE laser spike phenomena.

We have listed the 2-phenylbenzoxazole (PBO), which exhibits a prototypical standard ASE laser spike coinciding with the strongest Frank-Condon fluorescence vibronic band (Figure 6a), as a class 1 type (Table 1). Variation of driving laser energy from 3 to 24 mJ (at 266 nm, fourth harmonic of the Nd:YAG laser; cf. Figure 4 absorption spectrum) progressively suppresses the secondary ASE laser spike at 349 nm and dramatically enhances the primary ASE laser spike at 333 nm corresponding to the strongest Franck−Condon fluorescence vibronic band. The spectra of Figure 10 are for a 0.0054 M solution in methylcyclohexane at room temperature and are normalized to unit intensity at the 333 nm ASE laser spike. This is the standard behavior expected for ASE laser spike development for the simple fluorescence excitation case typical of most two-state/four-level molecular band lasers.

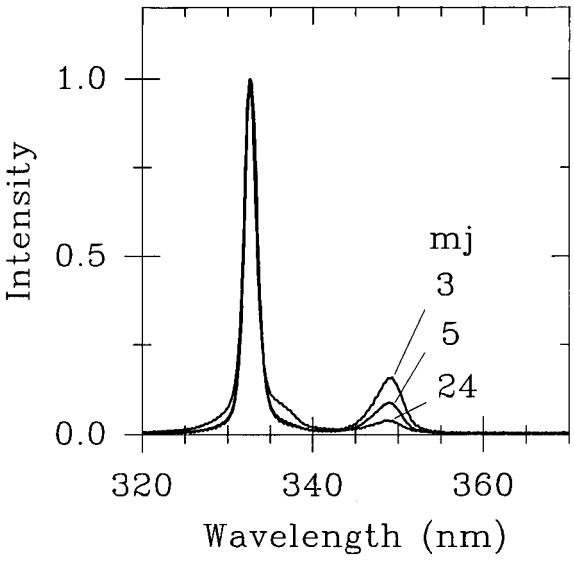

Figure 10. Normalized ASE spectra of 2-phenylbenzoxazole (0.0054 M) in methylcyclohexane. The ASE spike maxima are localized at 333 and 349 nm. With increasing the pumping energy at 266 nm from 3 to 24 mJ, the subsidiary ASE spike at 349 nm is getting more suppressed.

Comparison of the class 1 molecular behavior with the behaviors we have proposed in class 3 (Table 1) confirms the unorthodox behavior of the latter under the same variation of driving laser energy. The ASE laser spike development for α-NPD (0.0050 M in methylcyclohexane at room temperature) as the driving laser energy is raised from 4 mJ to 30 mJ is presented in Figure 11 (at 266 nm, fourth harmonic of Nd-YAG laser; cf. Figure 5 absorption spectrum). At 4 mJ driving laser energy, the ASE laser spikes simulate the corresponding prototype class 1 laser spike intensities, approximately parallel to the Franck−Condon fluorescence vibronic intensities (cf. Figures 5 and 8a).

Increasing the driving laser power immediately discriminates the class 3 behavior from the orthodox class 1 behavior, and the subsidiary band ASE laser spike developing rapidly as the laser spike corresponding to the strongest Franck−Condon fluorescence vibronic band rapidly decreases in relative magnitude. In this series for α-NPD, the extreme 30 mJ driving laser energy brings the two ASE laser spikes into essentially equivalent intensity (cf. Figure 8a).

The 2,5-diphenyloxazole (PPO) molecule exhibited the most extreme behavior as an unorthodox ASE laser spike case (Figure 9b). Figure 12 presents the studies of ASE laser spike development for 0.0051 M PPO in methylcyclohexane at room temperature. The driving laser energy varied from 0.6 to 32.6 mJ (266 nm, fourth harmonic of the Nd-YAG laser; cf. absorption spectrum for PPO in Figure 5), with the ASE laser spike intensities normalized to unit intensity at the 375 nm ASE laser spike, which corresponds to the subsidiary Franck−Condon fluorescence vibronic band (Figure 9a). The behavior demon-

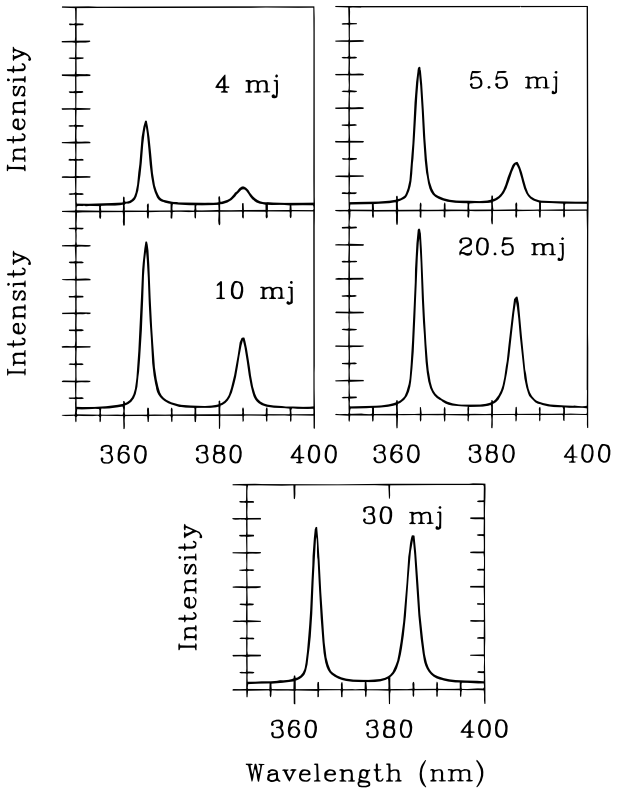

Figure 11. ASE spectra of the α-NPD molecule (0.0050 M) in methylcyclohexane at room temperature. The *y* axis has the same scale values for all the graphs in order to be compared from each other. When increasing the excitation energy at 266 nm from 4 to 30 mJ, the ASE spike localized at 385 nm has a larger increment of intensity compared to the ASE spike at 365 nm.

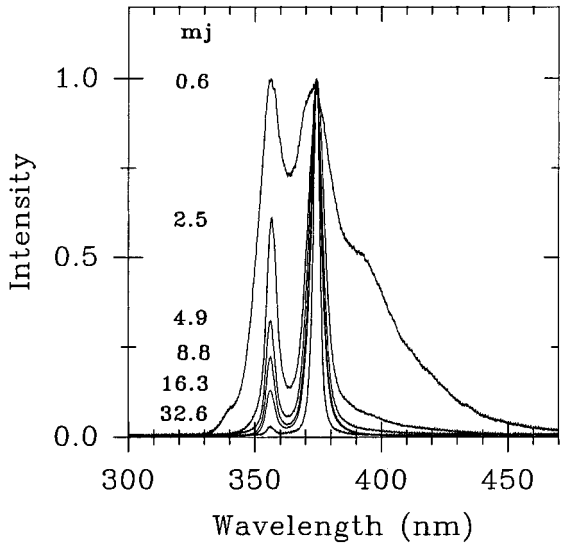

Figure 12. Fluorescence and ASE spectra of PPO (0.0051 M) in methylcyclohexane at room temperature. There is always a dominant spike at 374 nm. When increasing the energy pumping from 0.6 to 32 mJ, the laser spike at 356 nm is getting more suppressed. The emission spectra are normalized at their respective maxima.

strated in Figure 12 for PPO as a class 3 molecule is antithetical to that shown for PBO in Figure 10.

It is clear from the results of this section that ASE laser spike spectroscopy reveals excitation mode complexity not seen in ordinary absorption and fluorescence spectroscopy and that variation of driving laser energy offers a discriminating tool for further verifying the contrasting types of behavior revealed by ASE laser spectroscopy.

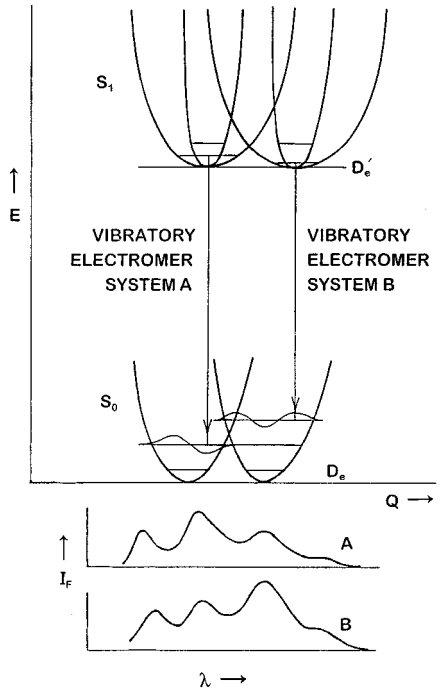

Figure 13. Schematic potential diagram, in the harmonic approximation, for the vibronic excitation soliton coupling between the molecular segments A and B of a heterocomposite molecule, with corresponding Franck−Condon electronic transition contours. In the S_1 state, the zero-point vibronic levels are shown for the lowest frequency normal mode and a high-frequency normal mode of A and B segments (Scheme 1).

8. The Spectroscopic Model for the ASE Laser Spike Anomalies of the Heterocomposite Molecules

The heterocomposite oxazoles of class 3 (Table 1), with unsymmetrical molecular segment A and B partitioning (Scheme 1), require a unique model to explain their unorthodox behavior in ASE laser spectroscopy. These molecules behave like ordinary molecules when judged by their equilibrium absorption and fluorescence spectroscopy: the relation between their lowest absorption and corresponding fluorescence bands is conventionally simple. However, in amplified spontaneous emission (ASE) laser spectroscopy, the molecules behave like a molecular mixture of two different species. Mixtures of lasing-capable molecules may reveal separate principal ASE laser spikes if the mixture exhibits resolved fluorescence peaks.[22] A further element of behavior which must be noted is that these two molecules, α-NPD and PPO (Table 1), show *constancy or independence of fluorescence spectrum with variations in excitation wavelength*. The definitive work of Saltiel's group[45] on molecular conformer spectroscopy shows the very subtle but resolvable variations in fluorescence band contour and position arising from molecular conformers of a given structure. The α-NPD molecule could exhibit such a conformer pair associated with a *syn*- and *anti*- disposition of the naphthyl ring, whereas for the PPO molecule, no molecular conformers of this type are conceivable. It may be emphasized that the electronic and vibronic envelope effects observed for ordinary aromatic molecular conformers are 1 or 2 orders of magnitude smaller than the effects that we have observed in ASE laser spectroscopy for both α-NPD and PPO. All of these facts have led us to postulate a special class of molecular conformers in order to account for the unorthodox strong ASE laser spike development some 1400 cm^{-1} from the normal laser spike expected at the strongest Franck−Condon fluorescence vibronic band.

The model we have developed has led to the construction of the dual potential diagram illustrated in Figure 13. We shall

SCHEME 2: Distances Corresponding to the Optimized Geometries of 2-Phenyloxazole, 5-Phenyloxazole in the S_o and S_1 States, and PPO in the S_o State

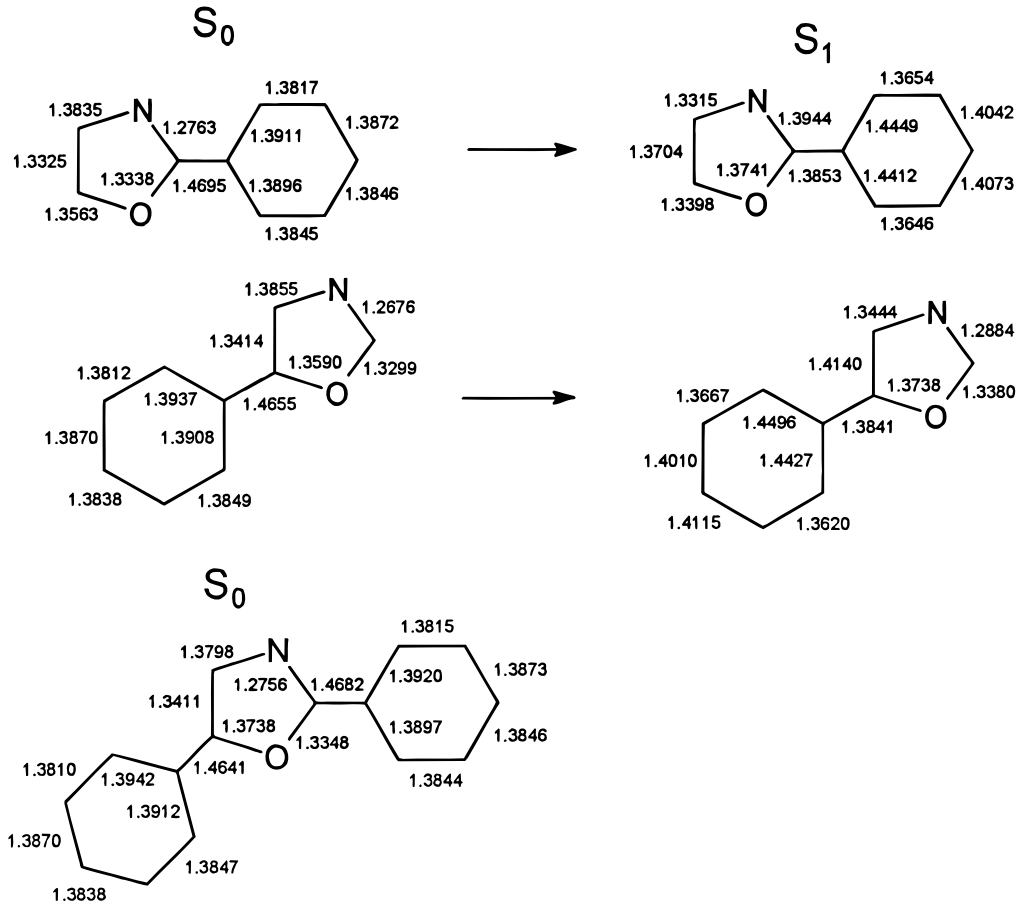

now correlate the distinctive features of this diagram with the structural and dynamical aspects of the *normal mode electromer* model we have defined. The electronic energies D_e for the S_o and S_1 states are taken as identical for the molecular segments A and B of our model (Scheme 1). For example, for α-NPD, in one electromer, segment A (5-phenyl-1,3,4-oxadiazole) is taken as a coplanar conjugated unit, which is slightly less strongly conjugated to the somewhat out-of-plane naphthyl ring, whereas, in the other *electromer*, segment B is the 2-(naphthyl)-1,3,4-oxadiazole as a coplanar conjugated unit, slightly less strongly conjugated with the 5-phenyl ring. In the segment A electromer features normal modes of the 5-phenyl-1,3,4-oxadiazole coplanar skeleton and the partitioned independent normal modes of the naphthyl ring. In the segment B electromer, the normal modes of the coplanar 2-(α-naphthyl)-1,3,4-oxadiazole skeleton now are active, and the partitioned independent normal modes of the 5-phenyl ring are mobilized.

It is then clear that the larger and more complex normal mode fragment will have a considerably lower average zero-point energy, and secondly, the vibrational entropy will be much greater for the more complex system.

Figure 13 schematically represents the concept of the Dushinsky[46] polyatomic Franck−Condon model (using parabolic potentials), where in the present case a low- and high-frequency vibrational mode potential is rotated into a coplanar diagram for each normal mode segment. In our representation of the model, the origins of the spectral transitions are unshifted, and the Franck−Condon intensities are electromer normal-mode-segment dependent. The model then offers the unique requirement of a constant electronic transition frequency with a change in position of the most intense Franck−Condon fluorescence peak. As a consequence, we could anticipate a shift of the ASE laser spike from the normal position at the dominant fluorescence vibronic band to a new position of a seemingly subsidiary band.

Overcoming the vibrational potential barrier constitutes the transfer of molecular distortion from segment A to segment B. For α-NPD, we consider that hydrodynamically, segment A would be favored in the ground state. In the nonequilibrium spectroscopic excitation, the large excess of vibrational energy would then be subject to a solitonic transfer of the associated molecular distortion from segment A to segment B. The soliton[47,48] is the concerted, unidirectional dominant distortion wave which in this case would be energetically and entropically driven. Such an effect reflects the excitation dynamics which is emphasized in the ASE laser spike phenomena with its enormous excited state population generation and with an initially huge excess of vibrational energy. In the equilibrated system involved in normal fluorescence, the segment A is dominant in the fluorescence envelope, and segment B transitions are hidden in the seemingly simple but disguised composite Franck−Condon envelope.

In the case of PPO, we recognize that the 2-phenyl ring coplanarity is favored as there is no steric barrier. The coplanarity is confirmed by our theoretical calculations. On the other hand, the proximate H-atoms (2 and 6 positions on the phenyl ring) of this 5-phenyl ring (oxazole numbering) will generate a steric potential with the oxazole ring 4-H position, thereby limiting coplanarity. We then would choose as the segment A conformer as that containing the coplanar 2-phenyloxazole normal mode fragment and the segment B conformer as that containing the hindered coplanar 5-phenyloxazole normal mode fragment, the latter representing low-frequency torsional modes for our model, and the odd phenyl ring 5 and 2 lying

TABLE 2: Inter-Ring Torsional Frequencies (cm^{-1}) in Phenyloxazoles

	2-phenyloxazole	5-phenyloxazole
ν_t (S_o)	51	11
ν_t (S_o)	134	118
	PPO	
	2-phenyl	5-phenyl
ν_t (S_o)	33.6	3.6

out of plane for segments A and B, respectively, and with decoupled normal modes with respect to the coplanar segments.

Theoretical Calculations. The chemical structure of the molecule PPO does not suggest simply the mechanical segments which could account for the anomalous ASE laser spike behavior. The partitioning of PPO into segments A and B which has been given is not obvious (Scheme 1). Segment B does not seem to be favored over segment A by an entropic criterion, in order for vibrational energy transfer to occur. Theoretical calculations (cf. Experimental Section) at the 6-31G** level for the S_o electronic state and at CIS 6-31G** level for S_1 yield some information that helps to unravel the driving path for energy transfer and suggests also the feasible normal mode electromer chemical structures.

The isolated 2-phenyloxazole and the 5-phenyloxazole molecules are both planar in the S_o and S_1 states by these calculations. Moreover, as Scheme 2 indicates, both structures as isolated molecules behave similarly in terms of bond-length changes upon excitation from state S_o to S_1. Especially noteworthy is the ring-joining C−C bond contraction in both 2-phenyloxazole and 5-phenyloxazole upon excitation, in contrast, to most of the internal ring-bond normal expansion upon excitation. For the complete PPO structure, only the S_o state geometry could be determined (lack of computer power), but the ring-joining C−C bond lengths are quite parallel to those of the isolated segment molecules, and we may surmise that analogous behavior would result for the S_1 state of PPO. Neither of these structural deductions shed much light on the excitation problem. Significant differences are however found if inter-ring torsional modes are analyzed. Table 2 presents theoretical data on the torsional frequencies of these molecular species under comparison.

As expected from the shortening bond lengths upon excitation, the inter-ring torsional frequencies increase with excitation from the S_o to the S_1 state. However, there is now evident a significant difference in torsional frequencies for the 2-phenyloxazole vs the 5-phenyloxazole molecules and molecular segments. As before, the S_1 state values for PPO were not calculable owing to insufficient computer memory.

The torsional energy barrier differences reflect the torsional frequency differences, as shown in Figure 14. It is seen that the inter-ring torsional barrier is significantly greater for the 2-phenyloxazole molecule than that for the 5-phenyloxazole isolated molecule, and these differences transfer to the molecular segments of the intact 2,5-diphenyloxazole molecule (PPO).

The torsional modes, especially for 5-phenyloxazole are so low that they would be strongly populated, with the 5-phenyloxazole representing many more quanta of torsional distortion. This at our present understanding would seem to provide the entropic driving force for the segment A → segment B vibrational energy transfer in the dynamics of excitation of PPO. Experimental femtosecond research could serve to expose other critical features in excitation mechanism of these cases.

9. Conclusion

It has been demonstrated that the various substituted phenyloxazoles studied (Table 1) can yield efficient amplified spontaneous emission (ASE) laser spikes in the ultraviolet, with gain coefficients reaching the high value of 10 cm^{-1} for our optical system. The presence of Franck−Condon resolved vibronic structure in the fluorescence bands permits highly resolved ASE laser spikes to be observed. These permit the study of unusual features of multiple-spike lasing, and give an insight to the chemical physics of excitation dynamics and the vibrational electronic interaction of these very complex polyatomic molecules. It is shown that anomalies arise for the asymmetric structures present in some of the phenyloxazoles, with dominant ASE laser spikes arising for nondominant fluorescence vibronic bands. In order to explain the anomalous ASE laser spike behavior, a spectroscopic potential model is introduced representing normal mode segments for an asymmetric molecular system with common electronic states. A solitonic transfer of the molecular distortion associated with the excess vibronic energy of the primary excitation is proposed as the intramolecular vibronic relaxation mechanism (IVR).

The variation of ASE laser spike development with driving laser energy, which represents increasing cycles of excitation, reinforces the concept of solitonic transfer of vibrational distortion from segment A to B (Scheme 1) as the first step in the excitation dynamics mechanism for intramolecular vibrational relaxation (IVR). In addition, the steady increase in the

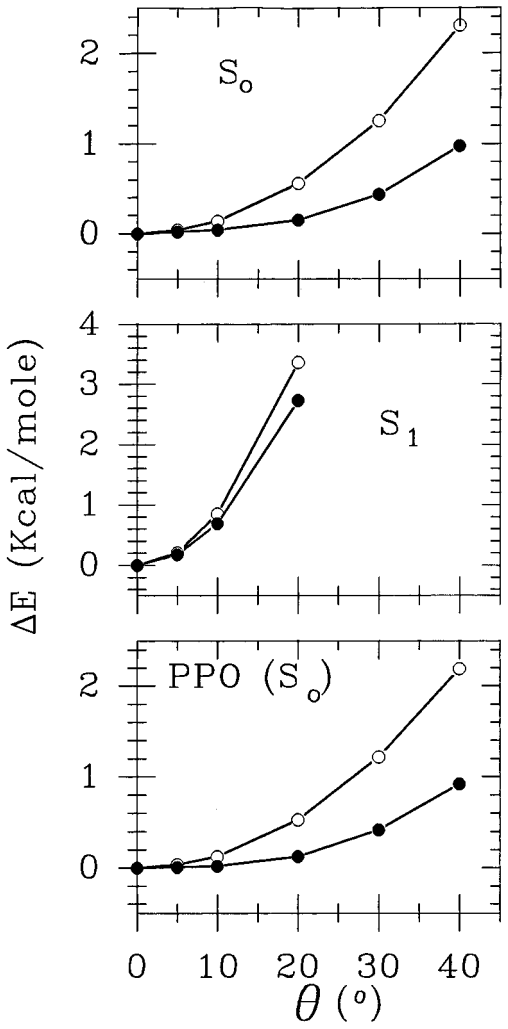

Figure 14. Torsional energy barrier increments (kcal/mol) relative to the planar conformation for 2-phenyloxazole (hollow circles) and 5-phenyloxazole (filled circles) either in the S_o or in the S_1 electronic states vs the inter-ring angle (θ, degrees) are shown above. The torsional energy barrier increments (kcal/mol) for PPO are plotted below vs the 2-phenyl and oxazole inter-ring angle (hollow circles) and vs the 5-phenyl and oxazole inter-ring angle (filled circles).

anomalous ASE laser spike intensity with driving laser energy can indicate intermolecular energy transfer in the excited state population inversion system. This is corroborated by the extraordinary relative intensities of the corresponding gain spectral peaks, which are superenhanced just in those cases in which the anomalously high ASE laser spike intensities are observed for the subsidiary Franck−Condon fluorescence vibronic bands.

We have used the gain coefficient $\alpha(\lambda)_L$ as an index of laser efficiency, following Shank (section IV).[3] By careful standardization of our optical bench arrangements and technique, we have achieved a high degree of reproducibility and believe that our gain coefficient measurements are a quantitative and reliable comparative index of the efficiency of the laser materials we have studied. A figure of merit index for laser dyes has been developed by Pavlopoulos[49] based on molecular optical parameters.

Altogether, the study of amplified spontaneous emission (ASE) laser spectroscopy can be seen to reveal inner details of excitation dynamics, not seen in ordinary equilibrium spectroscopy. In addition, the possibilities of probing these ultrafast events suggest new avenues for sub-picosecond spectroscopic researches.

Acknowledgment. The authors wish to thank the Spanish CICYT for financial support granted for the realization of this work as part of Project PB93-0280. We are please to acknowledge the valuable assistance in laser optics by Drs. L. van de Burgt and David A. Gormin of the IMB Laser Laboratory and the chemical nomenclature by Prof. Martin Schwartz. One of us (J.C.V.) acknowledges with thanks the granting of a Fulbright Scholarship by the Fulbright Commission and the Ministry of Education and Science of Spain. Mrs. Cristina Diaz is acknowledged for the gift of a sample of 2-phenyloxazole. We acknowledge with thanks the assistance of the staff of the magnetic resonance laboratory and Dr. R. Rosanske for recording the ^{13}C NMR spectra of α-NPD and PPO and his helpful comments. We thank Dr. J. R. Isasi for measuring the melting temperatures and for interesting discussions. Professor S. P. McGlynn of LSU gave stimulating input on the soliton model. We also thank Mr. I. V. Litvinyuk for helpful discussions of our paper, and Dr. N. G. Berloff for guiding us in the literature on soliton theory.

References and Notes

(1) Shank, C. V.; Dienes, A.; Silfvast, W. T. *Appl. Phys. Lett.* **1970**, *17*, 307.
(2) Lingel, C.; Kohn, R. L.; Shank, C. V.; Dienes, A. *Appl. Opt.* **1973** *12*, 2939.
(3) Shank, C. V. *Rev. Mod. Phys.* **1975**, *47*, 649.
(4) Dienes, A. *Appl. Phys.* **1975**, *7*, 135.
(5) Chou, P. T.; McMorrow, D.; Aartsma, T. J.; Kasha, M. *J. Phys. Chem.* **1984**, *88*, 4596.
(6) Del Valle, J. C.; Kasha, M.; Catalan, *J. Chem. Phys. Lett.* **1996**, *263*, 154.
(7) Rulliere, C.; Joussot-Dubien, *J. Opt. Commun.* **1978**, *24*, 38.
(8) Rulliere, C.; Denariez-Roberge, M. M. *Opt. Commun.* **1973**, *7*, 166.
(9) Broida, H. P.; Haydon, S. C. *Appl. Phys. Lett.* **1970**, *16*, 142.
(10) Furumoto, H. W.; Ceccon, H. L. *IEEE J. Quantum Electron.* **1970**, *QE-6* (5), 262.
(11) Lidholt, L. R.; Wladimiroff, W. W. *Opto-electronics (London)* **1970**, *2*, 21.
(12) Borisevich, N. A.; Gruzinskii, V. V.; Kutsyna, L. M. *Zh. Prikl. Spektrosk.* **1970**, *12*, 830 (English).
(13) Gruzinskii, V. V.; Danilova, V. I.; Kopylova, T. N.; Petrovich, P. I.; Shishkina, E. Yu. *Soviet Journal of Quantum Electronics* **1980** *10*, 678.
(14) Pavlopoulos, T. G.; Hammond, P. R. *J. Am. Chem. Soc.* **1974**, *96*, 6568.
(15) Abakumov, G. A.; Mestechkin, M. M.; Poltavets, V. N.; Simonov, A. P. *Soviet Journal of Quantum Electronics* **1978**, *8*, 1115.
(16) Maeda, M. *Laser Dyes: Properties of Organic Compounds for Dye Lasers*; Schäfer, F. P., Ed.; Academic Press: Inc., Orlando, FL, 1984.
(17) Drexhage, K. H. *Laser Dyes: Properties of Organic Compounds for Dye Laser*; Schäfer, F. P., Ed.; New York: Springer-Verlag, **1990**; Vol. 1 (Topics in Applied Physics).
(18) Sorokin, P. P.; Lankard, J. R. *IBMJ. Res. Dev.* **1966**, *10*, 162.
(19) Heldt, J. R.; Heldt, J. *Acta Phys. Pol. A* **1979**, *55*, 79.
(20) Kugel, R.; Svirmickas, A.; Katz, J. J.; Hindman, J. C. *Opt. Commun.* **1977**, *23*, 189.
(21) Hindman, J. C.; Kugel, R.; Svirmickas, A.; Katz, J. J. *Proc. Natl. Acad. Sci. U.S.A.* **1977**, *74*, 5.
(22) Chou, P. T.; Aartsma, T. J. *J. Phys. Chem.* **1986**, *90*, 721.
(23) Berlman, I. B.; Rokni, M.; Goldschmidt, C. R. *Chem. Phys. Lett.* **1973**, *22*, 458.
(24) Schäfer, F. P.; Bor, Zs.; Lüttke, W.; Liphardt, B. *Chem. Phys. Lett.* **1978**, *56*, 455.
(25) Spencer, R. D.; Weber, G. *Ann. N. Y. Acad. Sci.* **1969**, *158*, 361.
(26) (a) Frisch, M. J.; Trucks, G. W.; Schlegel, H. B.; Gill, P. M. W.; Johnson, B. G.; Robb, M. A.; Cheeseman, J. R.; Keith, T.; Petersson, G. A.; Montgomery, J. A.; Raghavachari, K.; Al-Laham, M. A.; Zakrzewski, V. G.; Ortiz, J. V.; Foresman, J. B.; Cioslowski, J.; Stefanov, B. B.; Nanayakkara, A.; Challacombe, M.; Replogle, E. S.; Gomperts, R.; Martin, R. L.; Fox, D. J.; Binkley, J. S.; Defrees, D. J.; Baker, J.; Stewart, J. P.; Head-Gordon, M.; Gonzalez, C.; Pople, J. A. *Gaussian 94*, Revision D.1.; Gaussian, Inc.: Pittsburgh, PA, 1995. (b) Spartan, Version 4.1; Wavefunction, Inc.: Irvine, CA, 1995.
(27) Foresman, J. B.; Head-Gordon, M.; Pople, J. A.; Frisch, M. *J. Phys. Chem.* **1992**, *96*, 135.
(28) Pople, J. A.; Scott, A. P.; Wong, M. W.; Radom, L. *Isr. J. Chem.* **1993**, *33*, 345.
(29) Heldt, J.; Gormin, D.; Kasha, M. *Chem. Phys.* **1989**, *136*, 321.
(30) Khan, A. U.; Kasha, M. *Proc. Nat. Acad. Sci. U.S.A.* **1983**, *80*, 1767.
(31) In our communication[6] we referred to this as a 3-level laser, focusing attention on the levels S_1, S'_o and S_o directly involved in the lasing action.
(32) Ricard, D.; Lowdermilk, W. H.; Ducuing, *J. Chem. Phys. Lett.* **1972**, *16*, 617.
(33) Catalan, J.; Mena, E.; Fabero, F.; Amat-Guerri, F. *J. Chem. Phys.* **1992**, *96*, 2005.
(34) Siegman, A. E. *Lasers*; Kelly, A., Ed. University Science Books: Mill Valley, CA, 1986.
(35) Kasha, M.; Sytnik A.; Dellinger, B. *Pure Appl. Chem.* **1993**, *65*, 1641.
(36) Levshin, W. L. *Acta Physchim. URSS*, **1935**, *2*, 221.
(37) Chou, P.-T.; Cooper, W. C.; Clements, J. H.; Studer, S. L.; Chang, C. P. *Chem. Phys. Lett.* **1993**, *216*, 2005.
(38) Davydov, A. S. *Theory of Molecular Excitons*; McGraw Hill, Book Co., Inc.: New York, 1962.
(39) McRae, E. G.; Kasha, M. *J. Chem. Phys.* **1958**, *28*, 721.
(40) Simpson, W. T.; Peterson, D. L. *J. Chem. Phys.* **1957**, *26*, 588.
(41) Kasha, M. *Radiat. Res.* **1963**, *20*, 55.
(42) McRae, E. G.; Kasha, M. *Physical Processes in Radiation Biology*; Augustine, L., Mason, R., Rosenberg, B., Eds.; Academic Press: New York, **1964**; p 23.
(43) Berlman., I. B. *J. Chem. Phys.* **1961**, *34*, 1083.
(44) Kutsyna, L. M.; Andryushchenko, O. I. *Zh. Prikl. Spektrosk.* **1975**, *22*, 255 (English).
(45) Saltiel, J.; Sears, D. F. Jr.; Choi, J.-O.; Sun, Y.-P.; Eaker, D. W. *J. Am. Chem. Soc.* **1994** *98*, 35.
(46) Dushinsky, F. *Acta Physicochim. URSS* **1937**, *7*, 551.
(47) Bullough, R. K., Cauchy, P. J., Eds.; *Topics in Current Physics*; Springer-Verlag; New York, 1980 (Solitons).
(48) Newell, A. C. *Solitons in Mathematics and Physics*; Society for Industrial and Applied Mathematics: Philadelphia, PA, 1985.
(49) Pavlopoulos, T. G. *Opt. Commun.* **1981**, *38*, 393.